Int. J. Heat Mass Transfer. Vol. 19, pp. 259–270. Pergamon Press 1976. Printed in Great Britain

THEORETICAL ANALYSIS OF A HORIZONTAL CONDENSER–EVAPORATOR TUBE

DAVID MOALEM* and SAMUEL SIDEMAN
Department of Chemical Engineering, Technion—Israel Institute of Technology, Haifa, Israel

(*Received* 1 *August* 1974 *and in revised form* 28 *May* 1975)

Abstract—The characteristics of the various parameters affecting the film side and overall heat-transfer coefficients in a horizontal evaporator–condenser were evaluated and presented for the laminar, and practically interesting, range of operating conditions. Comparison with the limited available experimental data show that the laminar theory yields transfer coefficients which are some 50 per cent of the experimental ones. However, when the effect of ripples is taken into account the calculated transfer coefficients conservatively predict, to within about 10–30 per cent accuracy, the performance of the evaporator–condenser tube.

NOMENCLATURE

A, heat-transfer surface;
B, x-dependent parameter ($= Co \sin X/2$);
Cp_1, specific heat of liquid;
Co, dimensionless constant ($= ReFr$);
c_i, constants ($i = 1 \ldots 10$);
D, inside tube diameter;
D_{is}, diffusion coefficient of inert in steam;
E_i, constants ($i = 1 \ldots 10$);
Fr, Froude number ($= gR/u_R^2$);
g, gravitation constant;
$h(x, z)$, local heat-transfer coefficient;
K, conductivities ratio (k_t/k_1);
K_z, Kapitza number ($= \mu^4 g/\rho\sigma^3$);
k_1, conductivity of liquid;
k_t, conductivity of tube material;
L, tube length ($= z_f$);
P^*, total pressure inside the tube;
P_v, vapor pressure in the external vapor chamber;
Pe, Peclet number ($= PrRe$);
Pr, Prandtl number ($CP_1\mu_1/k_1$);
Q_s, volumetric steam flow rate ($= Q_s(z)$);
$Q_s(0)$, inlet steam flow rate (at $z = 0$);
R, average tube radius;
$\hat{R}$, specific gas constant;
Re, Reynolds number ($= Ru_R\rho_1/\mu_1$);
R_i, inside tube radius;
R_0, outside tube radius;
r, radial coordinate;
S, vertical space between two successive tubes;
T^*, saturation temperature of steam, corresponding to P^*;
T_s, saturation temperature of steam at the condensate free surface ($= T_s(z)$);
T_v, saturation temperature of vapor, corresponding to P_v;
T_{wv}, T_{wc}, temperature of the tube wall surfaces on the evaporation–condensation sides;
ΔT^*, nominal temperature difference ($= T^* - T_v$);
ΔT_c, temperature difference ($= T_s - T_{wc}$);
$\Delta T(z)$, local temperature difference ($= T_s - T_v$);
$U(x, z)$, local overall heat-transfer coefficient;
$\bar{U}_i^*$, average overall heat-transfer coefficient (based on R_i);
U_c, U_v, dimensionless liquid velocities across the condensate and evaporating film;
u_c, u_v, dimensional liquid velocities across the condensate and evaporating film;
$\bar{u}_c, \bar{u}_v$, y-averaged liquid velocities across the condensate and evaporating film;
$\bar{u}_{v,0}$, initial (at $x = x_D$) y-averaged liquid velocity across the evaporating film;
u_R, reference velocity ($= \bar{u}_{v,0}$);
W_c, W_v, mass flow rates across the condensate and evaporating films;
x, tangential direction on the tube;
X, dimensionless tangential direction on the tube ($= x/R$);
x_D, initial peripheral distance for the evaporation region;
$\bar{x}_m$, final peripheral distance for the evaporation region;
y, normal coordinate on the tube (radial direction);
Y, dimensionless normal coordinate ($= y/R$);
y_c, condensate film thickness;
y_t, tube wall thickness;
y_v, evaporating film thickness;
$y_{v,0}$, initial film thickness ($x = x_D$);
z, axial coordinate of the tube;
z_f, final condensation length ($= L$).

Greek letters

Γ_v, Γ_c, liquid mass flow rates across the evaporating film and condensate;
$\Gamma_{v,0}$, initial liquid mass flow rate across the evaporating film;
γ, molar fraction of inerts;
$\gamma(0)$, inlet molar fraction of inerts (at $z = 0$);

*School of Engineering, Tel-Aviv University, Tel-Aviv, Israel.

δ_c, dimensionless condensate film thickness (y_c/R);
δ_t, dimensionless half tube wall thickness (y_t/R);
δ_v, dimensionless evaporating film thickness (y_v/R);
λ_v, λ_c, heat of evaporation and condensation in the evaporation–condensation sides;
θ, dimensionless temperature $((T-T_v)/(T^*-T_v))$;
θ_s, dimensionless temperature of the condensate free surface $((T_s-T_v)/\Delta T^*)$;
θ_{wv}, θ_{wc}, dimensionless temperature of the tube wall surfaces at the evaporation and condensation sides $((T_{wv}-T_v)/\Delta T^*$, and $(T_{wc}-T_v)/\Delta T^*)$;
μ_1, liquid viscosity;
ν_1, kinematic viscosity (μ_1/ρ_1);
ρ_1, liquid density;
ρ_s, steam density;
ϕ, angular coordinate;
σ, surface tension.

Subscripts

0, initial;
c, condensation side;
$i, 0$, inside and outside;
w, at the wall;
s, at the condensate free surface;
t, tube;
v, evaporation side.

INTRODUCTION

FILM-TYPE heat-exchangers show the distinct advantage of high heat-transfer coefficients and are utilized extensively in heating and cooling of liquids as well as in condensation and evaporation processes. Usually, vertical surfaces are used and, as in the case of the long tube evaporator (LTV), the evaporation which takes place inside the tube surface is sustained by the condensation of a saturated vapor on the external surface of the tube. Horizontal-tube-evaporator–condensers, where condensation takes place inside the tube bundle while the cooling evaporating film flows over the outside of the tubes (falling from one tube to the next below it), were recently shown [1–3] to have economical advantages over the classical vertical arrangements suggested in various water desalination schemes. The analysis of such an horizontal tube is the aim of this study.

As in most multi-stage water desalination plants, the vapor produced in one stage is condensed in the next stage. However, unlike the vertical case, condensation of the vapor inside the tube results in a two-phase flow, and the hydrodynamics of this two-phase flow determines the heat-transfer mechanism. A classification of the various flow regimes is given in [4, 5]. In the practical operating range considered, the condensation inside the tube can be classified by two condensate-flow regimes: stratified flow at $Re_v < 35000$ and annular flow at $Re_v > 35000$ [6]. In the stratified flow regime the condensation mechanism is predominantly affected by the viscous, inertial and body forces [7, 8], while in the annular flow regime the process of condensation is determined by the dynamics of the vapor and the condensate and their interaction [9–11]. As shown experimentally [12, 13], the condensation heat-transfer coefficient increases, in these two regimes, with steam flow rate.

Condensation on horizontal tubes was studied by a number of workers. At low temperature deriving forces and low vapor velocities, laminar film condensation occurs, and the Nusselt assumptions [14] for laminar film condensation on horizontal tube hold. Bromely [15] modified the Nusselt's model by investigating the contribution of the sensible heat term on the heat-transfer coefficient, other things being equal. For organic vapors, at high pressures and large temperature differences between the saturated vapor and the tube temperature, the effect of finite heat capacity of the condensate film is to increase the heat flow [15]. Rohsenow [16] includes the effect of "cross flow" of the heat transfer (convection in the flow direction) within the film, which was omitted in Bromely's analysis. Chen [17, 18] used an integral approach to the momentum and energy equations to improve the Nusselt's analysis. Sparrow and Gregg [19, 20] solved the problem by utilizing the boundary-layer type equations developed for the condensate layer on a horizontal tube. Koh, Sparrow and Hartnett [21] used the boundary-layer type equations but with a different set of boundary-conditions and obtained solutions quite similar to Chen's [18].

Condensation in inclined horizontal tubes was studied by some workers. The effect of the liquid accumulating inside the tubes at low mass velocities—and stratified flow of the condensate—was studied by Chaddock [22] and Chato [6]. Rufer and Kezios [7] extended these studies to higher steam flow rates. A detailed treatment for high steam flow rates resulting with annular flow within the tube was recently summarized by Rohsenow [23].

Very little has been reported on film flow on, and evaporation from, horizontal tubes. Zfati [24] studied heat transfer without evaporation to a film flowing over a horizontal tube and derived the tangential length of the developing thermal boundary layer. Fletcher *et al.* [29] reported experimental data for evaporation from a film flowing over a horizontal tube electrically heated from within. Also related is the study of evaporation from a film flowing on a near horizontal plane [25]. Wilkes [1] analysed the evaporating film outside a horizontal tube and the condensate film inside the tube as two independent phenomena. The local peripheral heat-transfer coefficient for the two films were evaluated based on the measured average constant value of the tube wall temperature. However, it often appears that the temperature measurements of the wall, and particularly at solid–fluid surfaces, are not sufficiently accurate [26].

None of the above studies consider the interrelated effects of the simultaneous evaporation–condensation

process, and practically all relate to a constant boundary condition at the wall. Nagendra and Tirunarayanan [36] utilize the laminar boundary layer approach to analyse film condensation on a non-isothermal vertical plate. The analysis, based on the arbitrarily assumed surface temperature distribution, indicates a decrease in the heat-transfer rate as compared to an isothermal assumption.

The present study is an attempt to solve for the heat-transfer rates associated with the interacting condensation and evaporation phenomena, while simultaneously solving for the wall temperature variation in the tangential and axial directions. The effect of the non-condensables in the condensing steam, along the tube, on the performance of the combined evaporation and condensation process is also considered.

THEORETICAL

The theoretical model and the governing equations

Consider an horizontal metal tube of wall thickness $2y_t$ and length L. Saturated steam at T^* enters the tube $z = 0$ and while flowing in the z direction condenses on the inside surface of the tube. The condensate film formed flows "down" in the tangential x-direction along the periphery of the tube. In the steam flow rates considered here ($Re_v < 35\,000$) the condensate forms a layer at the bottom of the tube. The external surface of the tube is continually wetted by a sheet of saturated (sea) water at T_v which falls on the tube at $x = 0$ (vertically) from above (perpendicular to the horizontal z-coordinate). A liquid film is thus formed on the external side of the tube flowing in the x-direction, and draining at the bottom of the horizontal tube. $T^* > T_v$ and the latent heat of condensation is utilized to evaporate some of the (sea) water film. The pressure in the vapor chest surrounding the tube is constant, corresponding to T_v. P^* is the total pressure corresponding to T^*.

A schematic presentation of the physical system and the coordinates used here is shown in Fig. 1. Figure 1(b) represents an angular cross section $\Delta\phi$ at some distance x from the upper stagnation point. Since x is defined along the perimeter, $\Delta x = R\Delta\phi$, and the angle of inclination varies with the distance x (from the vertical axis) along the periphery.

The thickness of the liquid films y_v and y_c, on the evaporation and condensation sides, respectively, is assumed to be small. The effect of curvature is neglected and a two-dimensional film flow is considered.

We now define the following dimensionless variables:

$$X = x/R, \quad Y = y/R, \quad \delta_v = y_v/R, \quad \delta_c = y_c/R,$$

$$\delta_t = y_t/R, \quad \theta = \frac{T - T_v}{T^* - T_v}, \quad \theta_s = \frac{T_s - T_v}{T^* - T_v}, \quad Re = \frac{u_R \rho_1 R}{\mu_1},$$

$$Pr = Cp_1\mu_1/k_1, \quad Fr = gR/u_R^2, \quad Co = FrRe,$$

$$U = u/u_R, \quad Pe = PrRe.$$

where T_s is the free surface temperature of the condensate. $T^* = T_s$ for pure steam and $T^* > T_s$ in the presence of non-condensables. u_R denotes a reference velocity to be determined later. U represents either U_c or U_v, constant properties are assumed throughout.

Neglecting the pressure gradient along the periphery of the tube, the dimensionless forms of the continuity, momentum and energy equations are:

$$\frac{\dot{m}_v}{\rho_1 u_R} = \frac{d}{dX}\int_{\delta_t}^{\delta_v} U_v\,dY; \quad \frac{\dot{m}_c}{\rho_1 u_R} = \frac{d}{dX}\int_{-\delta_t}^{\delta_c} U_c\,dY \tag{1}$$

$$\frac{d^2U}{dY^2} = -Co\sin X; \quad U = U_c \text{ or } U_v \tag{2}$$

$$Pe\frac{d}{dX}\int_{\delta_t}^{\delta_v} U_v\left(\theta - \frac{\lambda_v}{Cp_1\Delta T^*}\right)dY = -\left.\frac{d\theta}{dY}\right|_{Y=\delta_t}$$
$$Pe\frac{d}{dX}\int_{-\delta_t}^{\delta_c} U_c\left(\theta - \theta_s - \frac{\lambda_c}{Cp_1\Delta T^*}\right)dY = -\left.\frac{d\theta}{dY}\right|_{Y=-\delta_t} \tag{3}$$

where ΔT^* is the total nominal temperature driving force ($T^* - T_v$). (The temperature gradient inside the metal wall are considered below); $\dot{m}_v$ and $\dot{m}_c$ are the mass flux of the evaporating and condensing vapor, respectively.

The solution of the energy equations requires that the velocity and temperature profiles of the evaporating and condensing film be specified.

The velocity profiles

The velocity profiles are obtained by integrating the equations of momentum, assuming no slip conditions on the solid surfaces and no shear stresses on the free

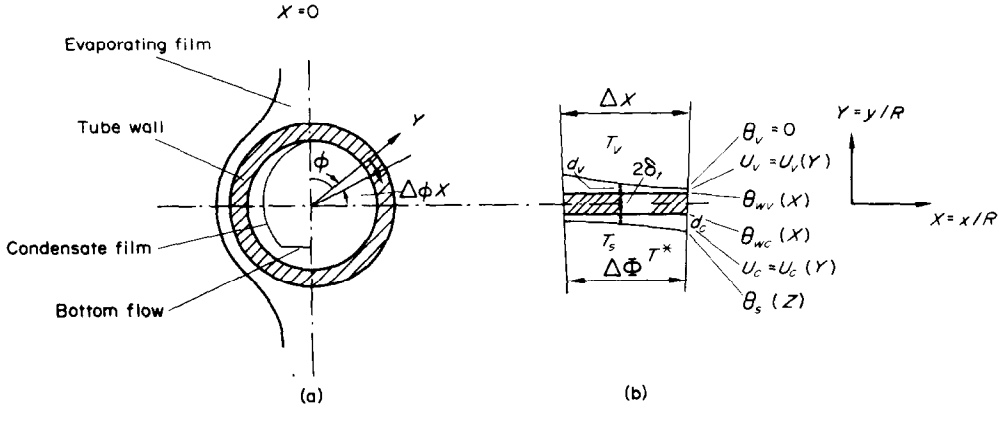

FIG. 1. Schematic presentation of the physical system and coordinates.

vapor–liquid interfaces of the two films. The neglect of the shear stress in the z-direction on the condensation side is justified for mild steam velocities (up to 50 ft/s) inside the tube [1]. As such, the following analysis is applicable to the stratified flow region of the Baker map [37].

The solution of equation (2) with these boundary conditions yields:

$$U_v = [-\delta_t(\delta_t+2\delta_v)+2(\delta_t+\delta_v)Y-Y^2]\frac{Co\sin X}{2}$$
$$U_c = [-\delta_t(\delta_t+2\delta_c)-2(\delta_t+\delta_c)Y-Y^2]\frac{Co\sin X}{2}. \quad (4)$$

The relationship between the (local) film thickness and the dimensionless flow rate W, evaluated by utilizing the local y-averaged (but x-dependent) velocity is given by:

$$W_v = \frac{\Gamma_v}{u_R\rho_1 R} = \tfrac{1}{3}\delta_v^3 Co\sin X$$
$$W_c = \frac{\Gamma_c}{u_R\rho_1 R} = \tfrac{1}{3}\delta_c^3 Co\sin X \quad (5)$$

wherefrom:

$$\frac{\dot m_v}{u_R\rho_1} = -\frac{dW_v}{dX} = \delta_v^2 Co\sin X\frac{d\delta_v}{dX}+\tfrac{1}{3}\delta_v^3 Co\cos X$$

and: (6)

$$\frac{\dot m_c}{u_R\rho_1} = +\frac{dW_c}{dX} = \delta_c^2 Co\sin X\frac{d\delta_c}{dX}+\tfrac{1}{3}\delta_c^3 Co\cos X\,.$$

Note that equations (5) are identical with the classical Nusselt's expression for the mass flow rate.

The temperature profiles

Linear temperature profiles are assumed for the two liquid films, as well as for the tube wall. Introducing the following boundary conditions

$Y=(\delta_v+\delta_t)$	$\theta=0$
$Y=\delta_t$	$\theta=\theta_{wv}$ (yet undetermined)
$Y=-\delta_t$	$\theta=\theta_{wc}$ (yet undetermined)
$Y=-(\delta_t+\delta_c)$	$\theta=\theta_s$ (= const. for pure vapor ≠ const. in presence of inerts)

(7)

yields:

$$\theta_v = \theta_{wv}\left(1+\frac{\delta_t}{\delta_v}\right)-\frac{\theta_{wv}}{\delta_v}Y$$
$$\theta_t = \frac{\theta_{wv}+\theta_{wc}}{2}-\frac{\theta_{wc}-\theta_{wv}}{2\delta_t}Y \quad (8)$$
$$\theta_c = \theta_{wc}\left(1+\frac{\delta_t}{\delta_c}\right)-\frac{\delta_t}{\delta_c}\theta_s-\frac{\theta_s-\theta_{wc}}{\delta_c}Y$$

θ_{wv} and θ_{wc}, which denote the dimensionless temperatures at the two sides of the wall, are also functions of X and are related to δ_v and δ_c by matching the fluxes in the $Y=\pm\delta_t$ planes:

$$-\left.\frac{d\theta_v}{dY}\right|_{Y=\delta_t} = -K\left.\frac{d\theta_t}{dY}\right|_{Y=\delta_t} \qquad K=\frac{k_t}{k_1}$$
$$-\left.\frac{d\theta_c}{dY}\right|_{Y=-\delta_t} = -K\left.\frac{d\theta_t}{dY}\right|_{Y=-\delta_t} \quad (9)$$

Differentiating (9) and rearranging (10) yields:

$$\theta_{wc} = \frac{2\delta_t+K\delta_v}{2\delta_t+K(\delta_v+\delta_c)}\theta_s \quad (10)$$

$$\theta_{wv} = \frac{K\delta_v}{2\delta_t+K\delta_v}\theta_{wc}. \quad (11)$$

Solution of the equations of energy

Combining the X-differentiated forms of (10) and (11) with the Y-integrated and X-differentiated forms of equations (5) and rearranging yields the variation of the film thickness in the X-direction

$$\frac{d\delta_v}{dX} = F_v(X,\delta_c,\delta_t,\delta_v,\theta_{wc},\theta_{wv},Re,Fr,Pr)$$
$$\frac{d\delta_c}{dX} = F_c(X,\delta_c,\delta_t,\delta_v,\theta_{wc},\theta_{wv},Re,Fr,Pr). \quad (12)$$

The exact form of equation (12) is presented in Appendix A.

Equations (12) represent a system of first order ordinary differential equations. A computer program was set for integrating the above system, starting with the initial values $\delta(X_0)$, using a Runge–Kutta-type method. The procedure performs on integration step and the results of each step serve as input for the next one. The stepsize is automatically controlled according to accuracy requirements and speed considerations.

The tangential integration range

The solution of equations (12) requires that the range of the independent variable X (over which the coupled integration proceeds) and the initial values of δ_c, and δ_v at X_0 be specified.

The initial values for the top of the tube. It is assumed that evaporation of the liquid film (which is saturated at the top of the tube) starts when the external free surface is affected by the thermal process (condensation) taking place inside the tube. This occurs when the thermal boundary layer is identical with the liquid film. The "developed boundary layer zone" is reached at a dimensional distance x_D (from the origin), which is given by [24]:

$$x_D = \frac{\sqrt{2}}{21{\cdot}25}\frac{\nu_1 Re_N}{u_g}\left(\frac{9}{128}Re_N+\frac{24{\cdot}24}{\pi}\right);$$
$$Re_N = \frac{4\Gamma_{v,0}}{\mu_1} \quad (13)$$

where $\Gamma_{v,0}$ is half the mass flow rate per unit length of the liquid falling on the tube; u_g is the film free fall velocity given by $\sqrt{(2gS)}$, and S is the vertical free fall distance, usually the vertical space between two tubes.

The dimensionless film thickness at x_D, $\delta_{v,0}$, is thus obtained from equation (5) where $\Gamma_v=\Gamma_{v,0}$ denotes the initial film mass flow rate per unit length.

Choosing the y-averaged velocity at $x=x_D$ as the reference velocity, i.e. $u_R=\bar u_{v,0}$, yields the relationship between Re (based on R) used here and $Re_N=4\Gamma_v/\mu_1$,

the Reynolds number commonly used in film flow studies:

$$Re \equiv \frac{u_R \rho_1 R}{\mu_1} = \frac{\Gamma_{v,0}}{\rho_1 y_{v,0}} \frac{\rho_1 R}{\mu_1} = \frac{1}{4\delta_{v,0}} Re_N. \quad (14)$$

The final values for the bottom of the pipe. In the operation range considered here, stratification of the condensate at the bottom of the horizontal tube occurs. The height of the condensate layer in the bottom is given in terms of the length averaged peripheral angle $\bar{X}_m$ by [22]:

$$\bar{X}_m = \pi - \left[5{\cdot}06 \times 10^{-4} \left(\frac{k_1^3 (\rho_1 - \rho_s) g}{\mu_1 \rho_1^3 \lambda_c^3} \right)^{3/4} \right]^{0{\cdot}142} \quad (15)$$

where D and L are the diameter and length of the tube, respectively. $\Delta T_c = T_s - T_{wc}$ is the temperature difference between the surface temperature of the condensate and the internal side of the wall. Since T_{wc} is not known *a priori*, the calculation is initiated by a reasonable guess and then corrected by an interaction procedure. The condensate level changes and X_m varies along the tube (by 3° for an 8 ft tube length [22]). Here we neglect this variation, and use is made of X_m, the L-averaged value of $\bar{X}_m$. As shown by Wilkes [1], the relative amount of heat transferred through the bottom layer, from $\bar{X}_m$ to π, is quite small and is assumed negligible here.

Utilizing equations (13) and (15), equations (12) are integrated to yield the local values of the two films around the periphery.

Condensation of pure vapor

Based on experimental observations [2], it may be assumed that the pressure drop along the tube is negligible. (This is particularly true for $T^* > 60°C$ and a relatively low heat flux.) Thus for pure steam, $T_s = T^*$ and $\theta_s = 1{\cdot}0$, invariant with the axial direction of the tube, and the equations presented thus are valid for any z along the tube. This assumption is substantiated by the fact that, unlike usual condensers, the external "cold" fluid falling on the tube in cross flow fashion is uniformly distributed along the tube and has a uniform homogeneous temperature.

With $\theta_s = 1$, the rate of condensation yields $\Gamma_{c,\bar{x}m}$, the (half periphery) accumulated condensate film flow rate per unit length of tube at the bottom ($X = \bar{X}_m$). Combining $\Gamma_{c,\bar{x}m}$ with a given steam inlet flow rate and exit steam quality yields the required tube length.

Effect of non-condensables

Non-condensables (usually air) are present in practically all condensing systems. The accumulation of non-condensables at the (fluid) condensation surface reduces the saturation pressure of the condensing steam and the corresponding saturation temperature T_s at the surface. As condensation proceeds along the tube, the effect of the inerts increases due to the reduction of the saturation temperature brought about by steam disappearance and the increased concentration of the inerts. T_s varies with the axial direction and henceforth denotes the local z-dependent temperature of the free surface of the condensate film. Condensation is halted as $T_s \to T_v$, the saturation temperature in the vapor chamber outside the tube. In the absence of inerts $T_s = T^*$. Thus, $(T^* - T_v)$ is the nominal driving force while $(T_s - T_v)$ is the effective one.

The relationship between the inert molar concentration fraction γ and the free surface temperature θ_s along the tube is now derived from simple thermodynamic relationships.

The partial pressure of the inerts at the wall is given by:

$$\begin{aligned} P_g(z, R) &= P^* \gamma(z, R); \quad R - y_c \simeq R \\ P_g(0, R) &= P^* \gamma(0, R) = P^* \gamma(0) \end{aligned} \quad (16)$$

since at the entrance γ is uniform, identical for all r. P^* is the total pressure within the tube, assumed constant along the tube. Condensation is halted at $z = z_f$, as $P_s(z_f, R)$, the partial pressure of the steam adjacent to the condensing surface, approaches P_v, the vapor pressure corresponding to the saturation temperature in the vapor chamber. Under these conditions $T_s \to T_v$ and

$$P_g(z_f, R) = P^* - P_s(z_f, R) \approx p^* - P_v. \quad (17)$$

Combining equations (16) and (17) yields:

$$\frac{\gamma(0)}{\gamma(z_f, R)} = \frac{P_g(0, R)}{P_g(z_f, R)} = \frac{P^*}{P^* - P_v} \gamma(0). \quad (18)$$

If a small nominal $\Delta T^* (= T^* - T_v)$ is considered, then by the Clausius–Clapeyron equation:

$$\frac{p^* - P_v}{P^*} = \frac{T^* - T_v}{\hat{R} T^{*2}} \lambda_c \quad (19)$$

where $\hat{R}$ is the specific gas constant.

Combining equation (18) with (19) yields the inerts concentration at which condensation stops:

$$\gamma(z_f, R) = \frac{\lambda_c}{\hat{R}} \frac{T^* - T_v}{T^{*2}}. \quad (20)$$

From small values of ΔT^*, a linear relationship between the temperature and vapor pressure can be assumed. The dimensionless free-surface temperature of the condensate is thus approximated by:

$$\theta_s(z) \equiv \frac{T_s(z) - T_v}{T^* - T_v} \simeq \frac{P_s(z, R) - p_v}{p^* - p_v}. \quad (21)$$

Introducing $P_s(z, R) = P^* - P_g(z, R)$ and $P_v = P^* - P_g(z_f, R)$ into (21) gives

$$\theta_s(z) = 1 - \frac{P_g(z, R)}{P_g(z_f, R)} = 1 - \frac{\gamma(z, R)}{\gamma(z_f, R)}. \quad (22)$$

As $\theta_s \to 0$, condensation stops. The length of the tube up to this point, z_f, can be determined once the concentration distribution of the inerts in the tube is known.

Homogeneous concentration of non-condensables occurs at high steam flow rates. Here, however, we limit the analysis to the intermediate range, where a completely mixed vapor phase exists, but stratification of the condensate, rather than an annular regime, still prevails. Under these stipulations, and assuming no

dissolution of the inerts in the condensate, the concentration of inerts at the free-interface are given by:

$$\gamma(z, R) = \frac{Q_s(0)}{Q_s(z)}\gamma(0) \tag{23}$$

and

$$\gamma(z_f, R) = \frac{Q_s(0)}{Q_s(z_f)}\gamma(0) \tag{24}$$

where $Q_s(z)$ is the steam flow rate at a distance z. Introducing (19) in (20) yields:

$$\frac{Q_s(0)}{Q_s(z_f)} = \frac{\lambda_c}{\hat{R}\gamma(0)}\frac{T^* - T_v}{T^{*2}}. \tag{25}$$

Combining equations (23) and (24) with (22) leads to the free surface temperature of the condensate along the tube for the assumed plug-flow case:

$$\theta_s(z) = 1{\cdot}0 - \left|\frac{Q_s(0)}{Q_s(z)} \Big/ \left(\frac{\lambda_c}{\hat{R}\gamma(0)}\frac{T^* - T_v}{T^{*2}}\right)\right|. \tag{26}$$

For relatively low steam loads, parabolic velocity and concentration distributions may be assumed (Appendix B) and the derived analogous expressions for the steam flow ratio and the condensate surface temperatures are:

$$\frac{Q_s(0)}{Q_s(z_f)} = 1 + \frac{1}{3}\left|\frac{\lambda_c}{\hat{R}}\frac{T^* - T_v}{\gamma(0)T^{*2}} - 1\right| \tag{27}$$

and

$$\theta_s(z) = 1 - \frac{[3Q_s(0)/Q_s(z) - 2/3]}{\dfrac{\lambda_c}{\hat{R}\gamma(0)}\dfrac{T^* - T_v}{T^{*2}}}. \tag{28}$$

Equations (25) and (27) are compared graphically for various operating conditions in Fig. 2.

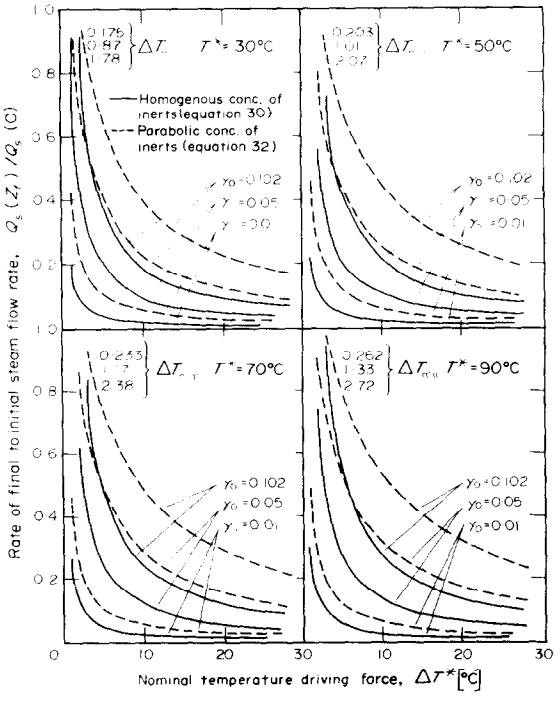

FIG. 2. Effect of non-condensables on condensation ratio as a function of the nominal temperature driving force.

As $\gamma(0)$ decreases, the ratio $Q_s(0)/Q_s(z_f)$ increases, i.e. the fraction of the inlet steam that condenses increases. Consequently a ratio of unity in equations (25) or (27) represents the limiting value for no condensation, and yields the minimum value of the nominal $\Delta T^*(= T^* - T_v)$ required to initiate condensation at the inlet, i.e.

$$\Delta T_{\min} = (T^* - T_v)_{\min} = \frac{\gamma(0)\hat{R}T^{*2}}{\lambda_c}. \tag{29}$$

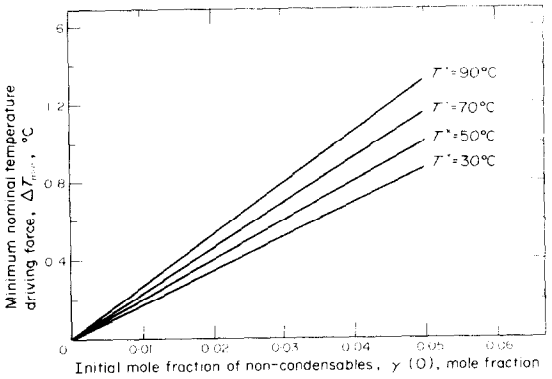

FIG. 3. Minimum temperature driving force required to sustain condensation in the presence of non-condensables.

Figure 3 represents the values of $\Delta T_{\min}$ corresponding to various saturation temperatures at various initial molar fractions of the inerts. Note that equation (29) is independent of the assumed concentration profile.

The heat-transfer coefficients

Utilizing equation (26) or (28), equations (12) can be solved for the tangential values of δ_c and δ_v as well as for the velocity and temperature profiles and the total and incremental mass flow rates of the two films. The local heat-transfer coefficient around the periphery at any z is obtained by:

$$h(x, z) = \frac{(\mathrm{d}q/\mathrm{d}t)}{\Delta T.\,\mathrm{d}A} = \frac{\lambda\,\mathrm{d}\Gamma}{\Delta T R\,\mathrm{d}\phi} = \frac{\lambda\mu}{R\Delta T}Re\frac{\mathrm{d}W}{\mathrm{d}X}; \qquad h = h_c \quad \text{or} \quad h_v \tag{30}$$

where ΔT denotes the local temperature difference across the condensate $(= T_s - T_{wc})$ or evaporating $(= T_{wv} - T_v)$ film, and $\mathrm{d}W/\mathrm{d}X$ denotes the local condensation or evaporation rate, equation (6).

With reference to the internal diameter of the tube the average overall heat transfer is defined by:

$$\overline{U_i}^* = \frac{\int_z \int_x U_i(x, z)\Delta T(x, z).\,\mathrm{d}A}{A\Delta T^*} \tag{31}$$

where $U_i(x, z)$ and $\Delta T(x, z)(= T_s - T_v)$ are the local values of the heat-transfer coefficient and temperature driving force, respectively. Equation (31) can similarly be related to the external diameter of the tube.

General outline of the solution procedure

Given the standard design data (T^*, T_v, $\gamma(0)$, $Q_s(0)$, etc.), we usually wish to determine the condensation and evaporation rate and consequently, the length of

the tube. The procedure, based on evaluating the local rates as affected by accumulating inerts along the tube, is as follows:

(a) Start at $z = 0$; $Q_s(0)/Q_s(z) = 1$ and solve (26), or (28), for $\theta_s(0)$.

(b) Utilizing $\theta_s(0)$, integrate equations (12) in steps, between the limits x_D and $\bar{x}_m$. This yields δ_c and δ_v, hence the velocity and temperature profiles; the tube-wall surface temperatures; the local liquid mass flow rates; the local condensation and evaporation rates and the heat-transfer coefficients.

(c) Step Δz in the axial direction. Calculate $Q_s(z)$ at the end of this step by:

$$Q_s(z) = Q_s(0) - \frac{2\Gamma_{c,\bar{x}m}}{\rho_s}\Delta z. \qquad (32)$$

(d) Utilize $Q_s(z)$ and repeat (a) i.e. solve for $\theta_s(z)$.

(e) Repeat (b) to (d) for $z = z + \Delta z$ till $\theta_s(z) \to 0$, (equations (26) or (28)). At this point $L = z_f$. For pure systems, $\theta_s(z) = 1$ at all z and the tube length is obtained as $Q_s(z)$ in equation (32) approaches zero. (In this case the length is determined by relating $\Gamma_{c,\bar{x}m}$ to the steam load.)

(f) Evaluate the average heat-transfer coefficients along the tube.

RESULTS AND DISCUSSIONS

Previous studies [9, 10, 13, 26] have usually been concerned with correlating the average values of the heat-transfer coefficient around the tube. The present study represents an attempt to predict the local and average values of the coefficients in the axial as well as in the peripheral directions, while accounting for the tube wall temperature variation. Since the solution is obtained numerically, it is interesting to note the characteristics and point values of the basic variables affecting the heat transfer coefficients at the condensation and evaporation surfaces.

Figure 4 represents the dimensionless internal and external temperatures around the periphery of the tube. With pure steam condensing inside the tube, some 80 per cent of the temperature drop occurs in the external evaporating film. As can be inferred from Fig. 3, the temperature drop across the evaporating and condensing film decreases in the presence of non-condensables. Under these conditions $\Delta T_{\min}$, the minimum nominal temperature difference required to maintain condensation, may constitute most of the available total driving force.

As demonstrated in Fig. 4, the driving force drop across the (aluminium) tube wall is relatively small. Since no condensate is assumed to exist at $x = 0$, the temperature difference across the wall at this point is minimal, i.e. $\theta_{wc} \to 1$ and θ_{wv} is very near unity due to the high ratio of the tube wall and the external film conductivities.

The variation of the dimensionless thickness of the condensate and the evaporating film along the periphery of the tube is presented in Fig. 5. Pure steam condensation is considered here, but the presence of

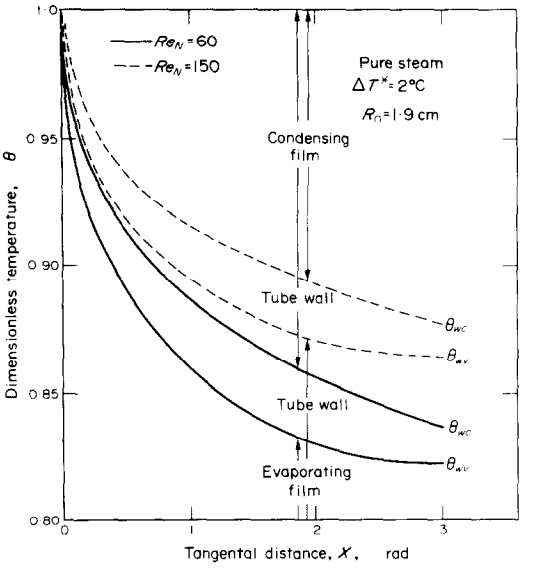

FIG. 4. Dimensionless temperature around the tube.

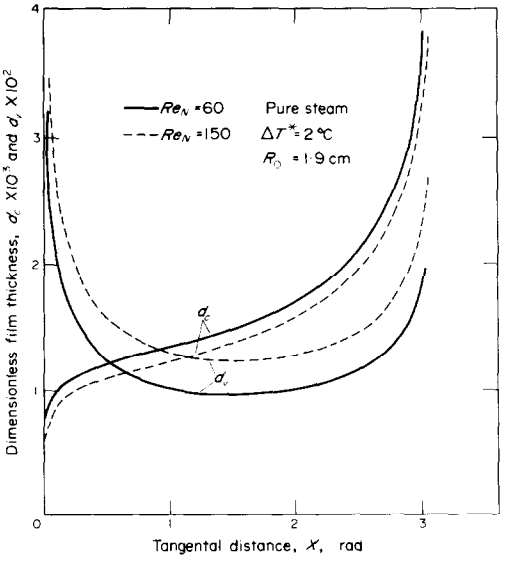

FIG. 5. Dimensionless film thickness around the tube.

inerts does not change the shape of the curves. In general, the effect of the angle of inclination on the evaporating film thickness is much more pronounced than that of the mass flow rate change due to mass transport from it and the film is thinnest at $\Pi/2$. The condensate film, on the other hand, starts to build up at the top and generally increases in thickness. However, the inflection point at $\Pi/2$ indicates the opposing effects of the mass flow rate change and the angle of inclination up to this point.

Figure 6 represents mass-transfer rates at the evaporation and condensation surfaces. The curves indicate a maximum mass flux near $\Pi/2$ where the films' thickness are at their lowest values. The evaporation rate is just slightly greater than the condensation rate. This is due to the fact that the effect of a heat capacity of the condensate and the evaporating films were not neglected [see equation (3)].

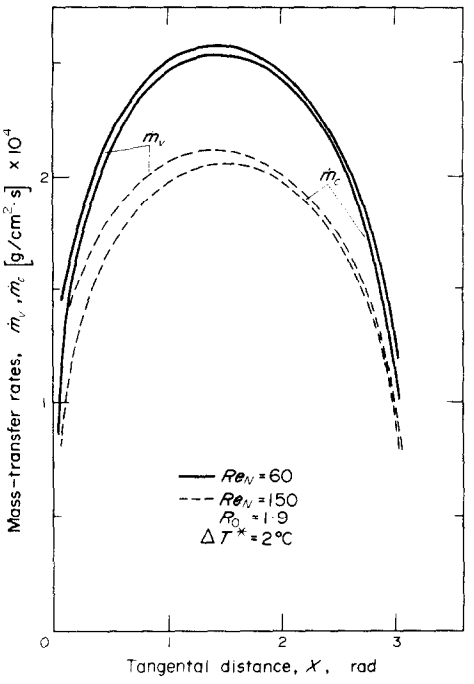

FIG. 6. Mass-transfer rate around the tube.

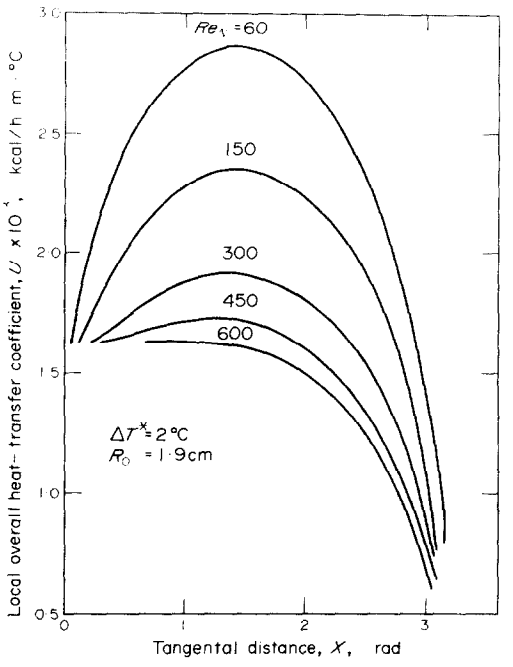

FIG. 8. Local overall heat-transfer coefficients around the tube.

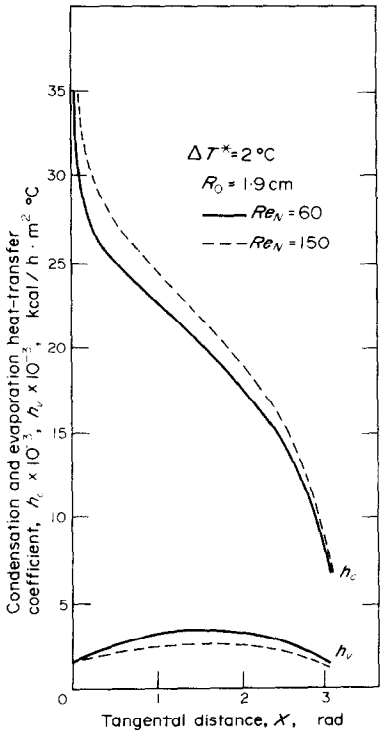

FIG. 7. Condensation and evaporation heat-transfer coefficients around the tube. Pure steam.

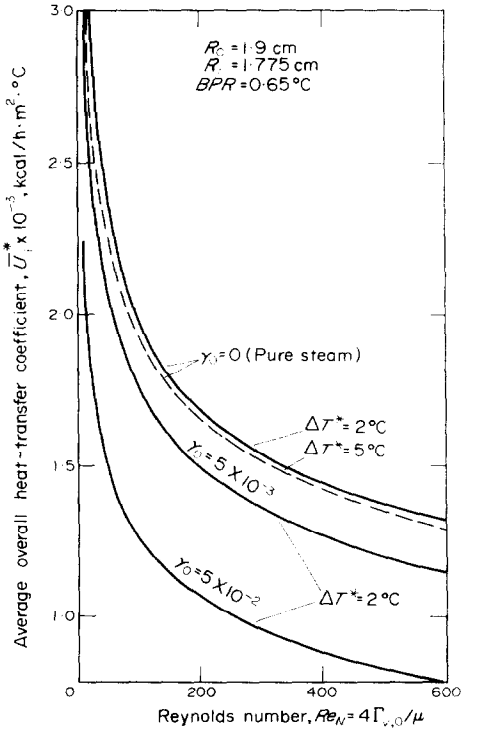

FIG. 9. Effect of non-condensables and ΔT^* on the heat-transfer coefficient.

The local evaporation and condensation heat-transfer coefficients calculated from the point values of the a.m. variables indicate a maximum in the evaporation side while a consistently decreasing function for the condensation side, Fig. 7. This is expected in view of the film thickness characteristics shown in Fig. 5. The local overall heat-transfer coefficient is presented in Fig. 8 for various values of the Reynolds number. The controlling effect of the evaporation side resistance is very pronounced. The decrease of the transfer coefficient with the Reynolds number in this range is further discussed below.

It is noteworthy that while the above relationships will change quantitatively if non-condensables are present in the condensing steam, their general characteristic will be preserved. The quantitative effects of these non-condensables are presented in Fig. 9. The assumed homogeneous distribution is applicable in the operating range dealt with here, and represents the case of least resistance in the condensation side. As is evident from Fig. 2, the parabolic profile presented here represents the limiting resitance, hence lowest transfer rates. However, in the flow range discussed here the transfer rate in the evaporating film is controlling the overall transfer rate, and the assumed concentration distribution of inerts will not greatly affect the results. Note, however, that at very low and high

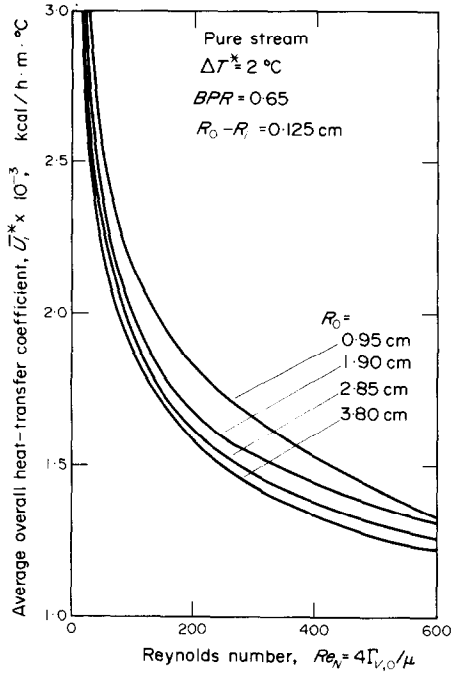

FIG. 10. Effect of Reynolds number on the average overall heat-transfer coefficient at various R_0. Pure steam.

flow rates of the external film, the overall transfer rate may be strongly affected by the condensate film.

Figure 9 represents the dependence of $\bar{U}_i^*$ on Re_N at various nominal (total) temperature driving forces. Increasing the Re_N at a constant ΔT^* in the laminar range discussed here corresponds to an increase of the (evaporating) film thickness. Since, as seen from Figs. 7 and 8, the external film coefficient is controlling the overall heat-transfer coefficient, increasing the Re_N number affects a decrease in $\bar{U}_i^*$. It must, however, be emphasized here that these theoretical calculations assume an evenly distributed film along the tube, whereas in practice the film is not uniformly distributed along the axis and, at the higher range of the Re_N values discussed here, the film is probably wavy. This deviation from uniformity would explain the reported experimental conclusion that the flow rate $\Gamma_{v,0}$ does not noticeably affect the average overall heat-transfer coefficient [1, 3]. Evidently, when $\Gamma_{v,0}$ is increased, "channelling" and local turbulence offset the effect of increasing the average film thickness.

As also seen in Fig. 9, increasing the nominal total temperature driving force causes a small decrease in $\bar{U}_i^*$. It is interesting to note that changing T^* (while keeping the ΔT^* constant) from 35 to 70°C did not appreciably affect $\bar{U}_i^*$. This is consistent with the experimental data of Tel Baruch [28] in which T_v varied from 30 to 55°C and the recent data of Fletcher *et al.* [29] in the range of 50–127°C.

The effect of the non-condensables present in the condensing steam is to reduce the temperature driving force. Hence, the effective temperature gradient between the evaporation chamber and the condensing steam is lower than the nominal difference between their corresponding saturation temperatures. The difference between the nominal and the effective driving forces is given by $\Delta T_{\min}$ in Fig. 3. With reference to Fig. 2 it is noteworthy that the effect of inerts on $\Delta T_{\min}$ is more pronounced at higher temperature levels.

Figure 9 also represents the effect of non-condensables, assumed to have homogeneous concentration profiles in the tube, on the heat-transfer coefficient. The effect of the inerts is more pronounced at lower ΔT^*s. Moreover, at small steam velocities, where a concentration profile of inerts is built up, some more severe effects of the non-condensables are expected at the back end of the tube.

The effect of the radius of the tube on the overall heat-transfer coefficient is presented in Fig. 10. Consistent with the simple Nusselt's derivation, $\bar{U}_i^*$ decreases as R increases.

A comparison of the theory presented here and experimental data is by necessity limited by the scarcity of available overall heat-transfer coefficients. The comparison is furthermore restricted to publications which include all the experimental variables required for the theoretical calculations.

Experimental transfer coefficients obtained in evaporation boiling of water films flowing over a horizontal tube electrically heated from within were recently reported by Fletcher *et al.* [29]. One and 2 in dia copper–nickel tubes were used, with heat fluxes varying from $1{\cdot}8 \times 10^4$ to $5{\cdot}4 \times 10^4$ kcal/h m². Re_N varied from 450 to 800 with saturation temperatures ranging from 50 to 125°C (3°C < ΔT^* < 9°C). The transfer coefficients varied between 4800 to about 9000 kcal/h m² °C.

Somewhat lower values of the overall heat-transfer coefficients (4300 kcal/h m² °C at $T^* = 50$°C and 5700 kcal/h m² °C at about 90°C) were obtained [2] with a horizontal tube-bundle operated with heat fluxes of about 2×10^4 kcal/h m².

As the theoretical model is limited to relatively low heat fluxes (i.e. relatively low steam flow rates and laminar films), a comparison with the above data is not possible. Also, the model presented here does not account for boiling.

A more meaningful comparison can be achieved by relating to data [28] obtained with evaporating–con-

densing tubes designed to operate at relatively low heat fluxes.

Table 1 represents data obtained from the experimental rig in Tel Baruch [28]. 1·5 in aluminium tubes, 122 cm long, were used, wetted from above by sea water. Temperature differences were obtained by measuring the pressure differences in the evaporating and condensing regions and correcting them for the boiling point elevation. Condensate flow rate was measured by collecting it from each tube separately. Sea water was not deaerated, and air content in the steam was determined to be between 100–150 ppm. Under these conditions, the effect of air is quite small.

Table 1. Comparison of experimental and calculated overall heat-transfer coefficients

Run	Re_N	ΔT^* [°C]	$\bar{U}_i^*$, [kcal/h m² °C] Experimental	Calculated	Modified by equation (33)
3-1	238·78	2·25	3017	1629	2043
3-2	224·91	2·51	3198	1643	2045
3-3	251·74	1·95	3016	1547	1954
6-1	235·72	2·00	3220	1707	2135
6-2	208·87	2·00	3331	1634	2013
6-3	207·84	2·20	2800	1691	2090
9-1	187·50	1·80	2835	1750	2135
9-2	190·91	1·70	3276	1791	2193
9-3	212·21	1·80	2922	1652	2045
VC-50	377·61	3·00	2150	1445	1905
VC-250	283·21	3·00	2350	1496	1913

As seen from Table 1, the calculated values are 30–45 per cent lower than the experimental ones. This is consistent with Chun and Seban's [30] study of evaporation on a vertical plate [30], which indicates that this deviation is due to the actions of ripples and waves. Indeed, Kapitza's relationship $Re_N = 2{\cdot}43Ka^{-1/11}$ [31] predicts that for the experimental system discussed here, capillary waves would form at the interface at $Re_N > 20$. Consequently, the average thickness of the film (for a given flow rate) at the operating conditions reported in Table 1 is smaller than calculated due to the presence of ripples and waves, and the actual heat-transfer coefficient is larger than the calculated one.

An empirical correction factor accounting for the increase of the condensation transfer coefficient due to rippling was suggested by Zazuli [32]:

$$\bar{h}_{\text{ripples}} = 0{\cdot}8\left(\frac{\Gamma}{\mu}\right)^{0{\cdot}11}\bar{h}_{\text{Nusselt}}. \qquad (33)$$

Applying Zazuli's correction to our calculated results, the deviations of the calculated values from the experimental data are reduced to 10–30 per cent. Unfortunately, an independent meaningful correlation of this variation is impossible with the limited data available at present.

Other effects may also contribute to the discrepancy between the experimental and calculated values. It is quite likely that the (sea) water is not uniformly spread along the tube. A fraction of the total area is covered by a relatively thin film whereas in other parts the flow is turbulent and/or wavy. Also, the non-uniform rain-like drops falling on the tube from the tube above it may enhance the transfer rate by initiating concentric waves. These effects are not accounted for by the theory.

Nusselt's analysis [14] indicates that the average condensing coefficient for a tube in an n-tube vertical bank is $n^{-1/4}$ times the average single-tube coefficient. The relatively high heat transfer rates for the lower tube in a vertical row [33, 34] have been attributed to the turbulence [35] or condensation on, and momentum gain [18] of, the accumulated condensate. However, Nusselt's analysis and its subsequent modifications [18, 35] for the multi-tube bundle relate to a significantly increasing condensate mass flowing outside the tubes. Here the fluid mass flowing outside the tubes varies relatively very little, as compared with the initial flow rate of the sea water flowing over the first tube. Thus, the present study can be considered as a reasonable approximation for the general case of the tube bundle.

CONCLUSIONS

The various parameters affecting the film-side and overall heat-transfer coefficients in a horizontal evaporator–condenser were evaluated and presented for a representative range of operating conditions. The controlling effect of the evaporation side film on the transfer rate was established. The effect of non-condensables present in underated sea water on the transfer rate in the flowing system treated here is quite small. This result seems to indicate that if proper measures are taken to vent the concentrated air stream leaving the tubes, thus avoiding accumulation of air in the system, deration of the incoming sea water may not be necessary.

Comparison with experimental data indicate that the theoretical analysis presented here for low heat flux operation underestimates the performance of a single evaporator condenser tube by about 30 per cent. Additional reliable experimental data is required in order to establish more firmly the accuracy of the theoretical predictions.

Acknowledgement—This study was sponsored by the Israel National Council for Research and Development. The authors wish to thank the Israel Desalination Engineering, Tel-Baruch Ltd., for their unlimited cooperation and the useful discussions with Mr. M. Pachter and Dr. A. Barak.

The writing of this report was interrupted by the War on the Day of Atonement. To our students and comrades in arms, whose valor, bravery, selfless humility and sacrifice allowed us to sit and write these words, we humbly dedicate this small contribution to human knowledge.

For water we toil. For peace we strive.

REFERENCES

1. Aqua-Chem, Inc., Research and development on the horizontal spray film evaporator, O.S.W. Rept. 209 (November 1966).
2. Universal Desalting Corp., Pilot plant tests and design study of a 2·5 MGD horizontal-tube multiple-effect plant, O.S.W. Rept. No. 492 (October 1969).
3. Universal Desalting Corp., Third report on horizontal tube multiple-effect process pilot plant tests, O.S.W. Rept. No. 740 (October 1971).
4. O. Baker, Simultaneous flow of oil and gas, *Oil Gas J.* **53**, 185 (1954).
5. K. J. Bell, J. Taborek and F. Fenoglio, Interpretation of horizontal in-tube condensation heat transfer correlation with a two-phase flow regime map, "Heat Transfer Minneapolis" 1969; *Chem. Engng Prog. Symp. Ser.* No. 102, **66**, 150 (1970).
6. J. C. Chato, Laminar condensation, *ASHRAE Jl* **4**, 52 (1962).
7. C. E. Rufer and S. O. Kezios, Analysis of two-phase, one component stratified flow with condensation, *J. Heat Transfer* **88C**, 265 (1965).
8. A. S. P. Sarma, P. K. Sarma and K. Vankata Apparao, An empirical correlation for condensation heat transfer under one-component stratified flow conditions, *Can. J. Chem. Engng* **50**, 541 (1972).
9. W. W. Akers, H. A. Deans and O. K. Corsser, Condensing heat transfer within horizontal tubes, *Chem. Engng Prog. Symp. Ser.* **55**(99), 171 (1959).
10. W. W. Akers and H. F. Rosson, Condensation inside a horizontal tube, *Chem. Engng Prog. Symp. Ser.* **56**(30), 145 (1960).
11. V. Narayama Murthy and P. K. Sarma, Condensation heat transfer inside horizontal tubes, *Can. J. Chem. Engng* **50**, 546 (1972).
12. H. F. Rosson and J. A. Myers, Point values of condensing film coefficients inside a horizontal pipe, *Chem. Engng Prog. Symp. Ser.* **61**(59), 190 (1965).
13. J. A. Myers and H. F. Rosson, Condensing coefficient inside a horizontal tube near atmospheric pressure, *Chem. Engng Prog. Symp. Ser.* **57**(32), 150 (1961).
14. W. Z. Nusselt, The surface condensation of steam, V.O.I. **60**, 541, 569 (1916).
15. L. A. Bromely, Effect of heat capacity of condensate, *Ind. Engng Chem.* **44**, 2966 (1952).
16. W. M. Rohsenow, Heat transfer and temperature distribution in laminar film condensation, ASME Paper No. 54-A-144 (1954).
17. M. M. Chen, An analytical study of laminar film condensation: Part 1: flat plates, *J. Heat Transfer* **83C**, 48 (1961).
18. M. M. Chen, An analytical study of laminar film condensation: Part 2: single and multiple horizontal tubes, *J. Heat Transfer* **83C**, 55 (1961).
19. E. M. Sparrow and J. L. Gregg, A boundary layer treatment of laminar film condensation, *J. Heat Transfer* **81C**, 13 (1959).
20. E. M. Sparrow and J. L. Gregg, Laminar condensation heat transfer on a horizontal cylinder, *J. Heat Transfer* **81C**, 291 (1959).
21. J. C. Y. Koh, E. M. Sparrow and J. P. Hartnett, The two-phase boundary layer in laminar film condensation, *Int. J. Heat Mass Transfer* **12**, 69 (1969).
22. J. B. Chaddock, Film condensation of vapor in a horizontal tube, *Refrig. Engng* **65**, 36, 90 (1957).
23. W. M. Rohsenow, in *Handbook of Heat Transfer*, edited by W. M. Rohsenow and J. P. Hartnett, Section 12, pp. 12–19. McGraw-Hill, New York (1973).
24. A. Zfati, Heat transfer in laminar flow of a liquid film on a horizontal cylinder (in Hebrew), M.Sc. Thesis, Dept. Mech. Eng., Technion—Israel Inst. of Technology, Haifa, Israel (1971).
25. A. Gollan and S. Sideman, Direct contact heat transfer with change of phase: co-current flow of immiscible films with surface evaporation, *Int. J. Heat Mass Transfer* **11**, 1761 (1968).
26. H. Groothuis and W. P. Handal, Heat transfer in two-phase flow, *Chem. Engng Sci.* **11**, 212 (1959).
27. A. E. Dukler and L. C. Elliott, Experimental and analytical studies of heat transfer in a falling film system, O.S.W. Rept. No. 287 (1967); also personal communication (1973).
28. Development of horizontal evaporation—condenser desalination unit, Desalination Engineering Ltd., Tel-Baruch, Internal Report (1973).
29. L. S. Fletcher, V. Sernas and L. S. Galowin, Evaporation from thin water films on horizontal tubes, *Ind. Engng Chem. Process Des. Dev.* **13**, 265 (1974).
30. K. R. Chun and R. A. Seban, Heat transfer to evaporating liquid films, *J. Heat Transfer* **93**, 391 (1971).
31. A. E. Dukler, Fluid mechanics and heat transfer in vertical-film systems, *Chem. Engng Prog. Symp. Ser.* **56**(30), 1 (1960).
32. W. Wilke, Wärmeübergang en Rieselfilme, V.D.I. Forschungsheft 490 (1962).
33. F. L. Young and W. J. Wohlenberg, Condensation of saturated Freon-12 vapor on a bank of horizontal tubes, *Trans. Am. Soc. Mech. Engrs* **64**, 787 (1942).
34. D. L. Katz and J. M. Geist, Condensation on fixed finned tubes in a vertical row, *Trans. Am. Soc. Mech. Engrs* **70**, 907 (1948).
35. D. Q. Kern, Mathematical development of tube loading in horizontal condensers, *A.I.Ch.E. Jl* **4**(2), 157 (1958).
36. H. R. Nagendra and M. A. Tirunarayanan, Laminar film condensation from nonisothermal vertical flat plates, *Chem. Engng Sci.* **25**, 1073 (1970).

APPENDIX A

Equation (14)

The exact form of equation (14) is given by

$$\frac{d\delta_v}{dX} = \frac{E_9/Pe_c - C_8/Pe_v - E_9C_{10} + E_{10}C_9}{E_9C_8 - E_9C_8}$$
$$\frac{d\delta_c}{dX} = \frac{E_8/Pe_c - C_8/Pe_v - E_8C_{10} + E_{10}C_8}{E_8C_9 - E_9C_8} \quad (14a)$$

where:

$$E_8 = [2BE_5\delta_v^3 + \tfrac{2}{3}BE_6\delta_v^4 - B\theta_{wv}(\tfrac{5}{4}\delta_v^3 + \tfrac{4}{3}\delta_t\delta_v^2) - BE_3(\tfrac{5}{\Gamma 2}\delta_v^4 + \tfrac{2}{3}\delta_t\delta_v^3)]/\theta_{wv}$$

$$E_9 = [\tfrac{2}{3}BE_7\delta_v^4 - BE_4(\tfrac{5}{\Gamma 2}\delta_v^4 + \tfrac{2}{3}\delta_t\delta_v^3)]/\theta_{wv}$$

$$E_{10} = [\tfrac{2}{3}E_5\delta_v^4 - \theta_{wv}(\tfrac{5}{\Gamma 2}\delta_v + \tfrac{2}{3}\delta_t\delta_v^3)]\frac{dB}{dX}\Big/\theta_{wv}$$

$$E_1 = K\delta_v \quad E_2 = 2\delta_t + K\delta_v \quad E_5 = \theta_{wv}\left(1 + \frac{\delta_t}{\delta_v}\right) - \frac{\lambda_v}{C_p\Delta T^*}$$

$$E_3 = 2\delta_t K\theta_{wc}/E_2^2 + C_3E_1/E_2 \quad E_6 = -\frac{\delta_t}{\delta_v^2}\theta_{wv} + \left(1 + \frac{\delta_t}{\delta_v}\right)E_3$$

$$E_4 = C_4E_1/E_2 \quad E_7 = \left(1 + \frac{\delta_t}{\delta_v}\right)E_4$$

$$C_8 = [\tfrac{2}{3}BC_6\delta_c^4 + BC_3(\tfrac{5}{12}\delta_c + \tfrac{2}{3}\delta_t\delta_c^3)](\theta_s - \theta_{wc})$$

$$C_9 = [2BC_5\delta_c^5 + \tfrac{2}{3}BC_7\delta_c^4 - B(\theta_s - \theta_{wc})(\tfrac{5}{4}\delta_c^4 + \tfrac{4}{3}\delta_c^3\delta_t) + BC_4(\tfrac{5}{12}\delta_c^4 + \tfrac{2}{3}\delta_t\delta_c^3)]/(\theta_s - \theta_{wc})$$

$$C_{10} = [\tfrac{2}{3}C_5\delta_c^4 - (\theta_s - \theta_{wc})(\tfrac{5}{12}\delta_c^4 + \tfrac{2}{3}\delta_t\delta_c^3)]\frac{\mathrm{d}B}{\mathrm{d}X}/(\theta_s - \theta_{wc})$$

$$C_1 = (2\delta_t + K\delta_v)\theta_s \qquad C_5 = (\theta_s - \theta_{wc})\left(1 + \frac{\delta_t}{\delta_c}\right) + \frac{\lambda_c}{C_p\Delta T^*}$$

$$C_2 = 2\delta_t + K(\delta_v + \delta_c) \qquad C_6 = \left(1 + \frac{\delta_t}{\delta_c}\right)C_3$$

$$C_3 = K(C_2\theta_s - C_1)/C_2^2 \qquad C_7 = \left(1 + \frac{\delta_t}{\delta_c}\right)C_4 - \frac{\delta_t}{\delta_c^2}(\theta_s - \theta_{wc})$$

$$C_4 = -KC_1/C_2^2 \qquad B = \tfrac{1}{2}Co\sin X.$$

APPENDIX B

Parabolic Concentration Distribution of Inerts Associated with Low Steam Loads

Parabolic profiles for the steam velocity and the concentration of inerts are assumed in the steam core. Moreover, the migration of steam towards the free-condensate surface has but a little effect on the parabolic nature of these profiles [27].

The boundary conditions are, for all z:

$$r = 0 \quad D_{is}\frac{\mathrm{d}v}{\mathrm{d}r} = 0; \qquad \frac{\mathrm{d}\gamma}{\mathrm{d}r} = 0; \qquad \gamma = \gamma_0 \tag{B1}$$

$$r = R \quad v = 0; \qquad -D_{is}\frac{\mathrm{d}\gamma}{\mathrm{d}r} = 0 \tag{B2}$$

where D_{is} denotes the diffusion coefficient of inerts in steam and v is the steam velocity.

The first two B.C. are self-evident due to symmetry. The prescribed value of concentration at $r = 0$ implies that within the relatively short condensation period, and based on the laminar regime of flow, the concentration in the center-line of the tube remains constant, at the initial inlet concentration. Moreover, for small steam velocities, the no-slip condition for the axial velocity at the condensate free surface is quite reasonable. The last B.C. states that the condensate is impermeable to the inerts. Neglecting the volume occupied by the condensate film within the tube, and assuming that the change in the average molecular weight along the tube is negligible:

$$Q_s(z)\rho_s = \int_0^R \rho_s v(z, r)2\pi r\,\mathrm{d}r \tag{B3}$$

$$Q_s(0)\rho_s\gamma(0) = \int_0^R \gamma(z, r)\rho_s v(z, r)2\pi r\,\mathrm{d}r. \tag{B4}$$

Solving (B3) and (B4) with the appropriate boundary conditions yields

$$v(z, r) = \frac{2Q_s(z)}{\pi R^2}\left(1 - \frac{r^2}{R^2}\right) \tag{B5}$$

$$\gamma(z, r) = \gamma(0)\left[1 + 3\left(\frac{Q_s(0)}{Q_s(z)} - 1\right)\left(\frac{r}{R}\right)^2\right]. \tag{B6}$$

For $r = 0$ $\gamma(z, r) = \gamma(0)$.

Thus, for $0 < z < z_f$ we note that $Q_s(z_f) < Q_s(z) < Q_s(0)$ and $\gamma(0) < \gamma(z, R) < \gamma(z_f, R)$, consistent with physical reality.

ETUDE THEORIQUE D'UN TUBE CONDENSEUR-EVAPORATEUR HORIZONTAL

Résumé—On a évalué et présenté les caractéristiques des divers paramètres qui affectent le film et les coefficients de transfert globaux dans un évaporateur-condenseur horizontal, pour des conditions opératoires qui correspondent au cas laminaire pratiquement intéressant. La comparaison avec les données expérimentales disponibles, mais limitées, montre que la théorie laminaire fournit des coefficients de transfert moitié moindre que ceux expérimentaux. Cependant, lorsque l'on tient compte de l'effet des rides, les coefficients de transfert calculés prédisent à peu près, avec une précision de l'ordre de 10 à 30 pour cent, le fonctionnement du tube évaporateur-condenseur.

THEORETISCHE ANALYSIS EINES HORIZONTALEN KONDENSATOR-VERDAMPFERROHRES

Zusammenfassung—Der Einfluss verschiedener Parameter auf die filmseitigen und Gesamtwärmeübergangskoeffizienten in einem horizontalen Kondensator-Verdampferrohr wurden berechnet und für laminare und praktisch interessierende Arbeitsbedingungen angegeben. Der Vergleich mit den beschränkt verfügbaren experimentellen Werten zeigt, dass die laminare Theorie Wärmeübergangskoeffizienten liefert, die etwa 50% der experimentellen betragen. Wird jedoch der Einfluss von Wellen berücksichtigt, dann geben die berechneten Wärmeübergangskoeffizienten das Verhalten von Kondensator-Verdampferrohren innerhalb von 10–30% wieder.

ТЕОРЕТИЧЕСКИЙ АНАЛИЗ ГОРИЗОНТАЛЬНОЙ ИСПАРИТЕЛЬНО-КОНДЕНСАЦИОННОЙ ТРУБЫ

Аннотация — Для представляющих практический интерес ламинарных режимов течения рассчитаны и приведены характеристики различных параметров, влияющих на коэффициент теплоотдачи со стороны пленки и суммарный коэффициент теплопереноса в испарительно-конденсационной трубе. Сравнение с имеющимися немногочисленными экспериментальными данными показывает, что теоретически найденные коэффициенты переноса совпадают с экспериментальными в пределах 50%. Однако, в случае учета влияния пульсаций расчетные коэффициенты переноса позволяют определить режимы работы испарительно-конденсационной трубы с точностью примерно до 10–30%.